JUSTC

Article

http://justc.ustc.edu.cn

Received: April 14, 2022; Accepted: May 10, 2022

Three-dimensional tubular carbon aerogel for supercapacitors

Qiguo Shang*, Jie Xu*, and Jianwei Liu ✉

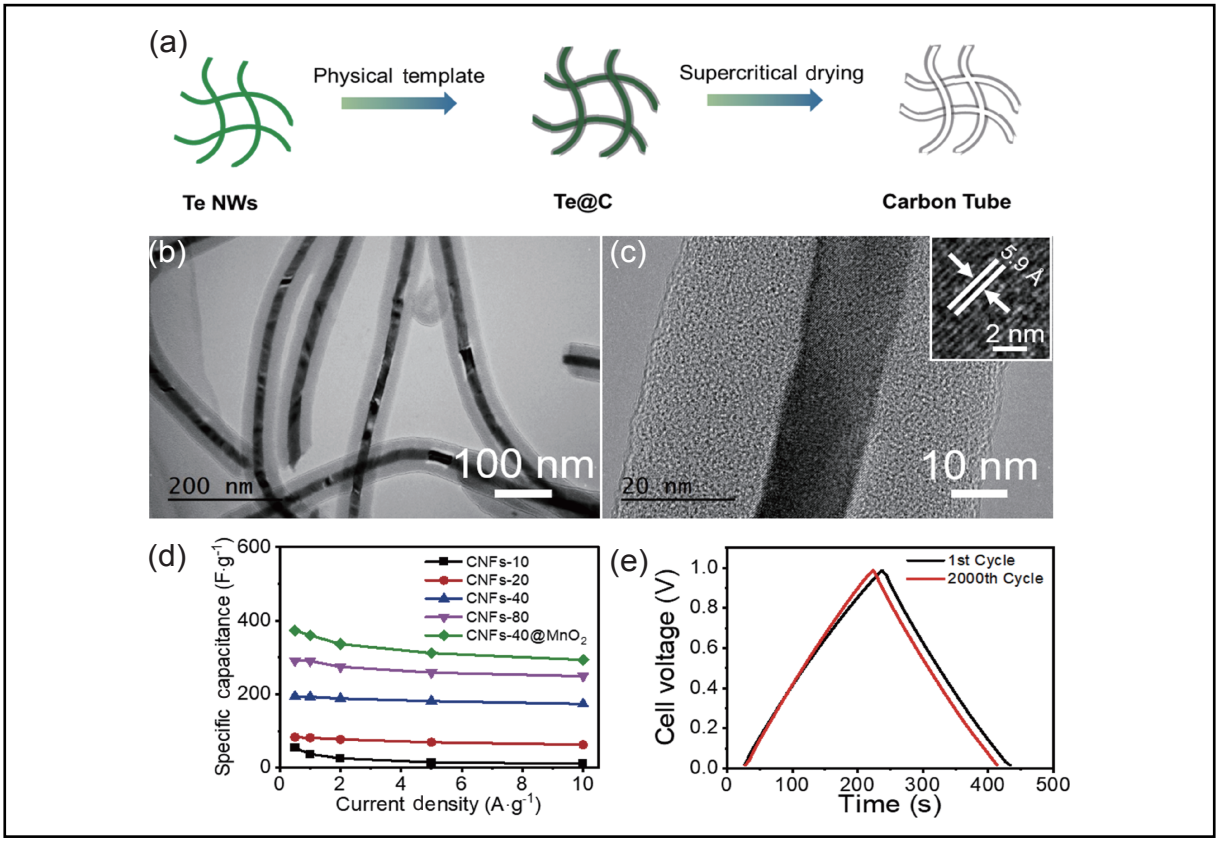
Department of Chemistry, Institute of Biomimetic Materials & Chemistry, Anhui Engineering Laboratory of Biomimetic Materials, Division of Nanomaterials & Chemistry, Hefei National Research Center for Physical Sciences at the Microscale, Institute of Energy, Hefei Comprehensive National Science Center, University of Science and Technology of China, Hefei 230026, China

* These authors contributed equally to this work

✉Correspondence: Jianwei Liu, E-mail: jwliu13@ustc.edu.cn

© 2022 The Author(s). This is an open access article under the CC BY-NC-ND 4.0 license (http://creativecommons.org/licenses/by-nc-nd/4.0/).

Graphical abstract



Carbon nanotube gels with large specific surface areas are promising for use as electrode materials for supercapacitors.

Public summary

- Elastic carbon nanotube aerogels were fabricated via a simple hydrothermal-carbonization process using the Te NWs as the sacrificial template.
- The inner diameter of the carbon tube can be controlled by controlling the diameter of the tellurium nanowires.
- The unique properties of the hollow structure provide carbon nanotubes with better capacitive performance and cycling stability.

Citation: Shang Q G, Xu J, Liu J W. Three-dimensional tubular carbon aerogel for supercapacitors. *JUSTC*, **2022**, 52(8): 6. DOI: 10.52396/JUSTC-2022-0065

JUSTC

Article

http://justc.ustc.edu.cn

Received: April 14, 2022; Accepted: May 10, 2022

Three-dimensional tubular carbon aerogel for supercapacitors

Qiguo Shang*, Jie Xu*, and Jianwei Liu ✉

Department of Chemistry, Institute of Biomimetic Materials & Chemistry, Anhui Engineering Laboratory of Biomimetic Materials, Division of Nanomaterials & Chemistry, Hefei National Research Center for Physical Sciences at the Microscale, Institute of Energy, Hefei Comprehensive National Science Center, University of Science and Technology of China, Hefei 230026, China

* These authors contributed equally to this work

✉Correspondence: Jianwei Liu, E-mail: jwliu13@ustc.edu.cn

© 2022 The Author(s). This is an open access article under the CC BY-NC-ND 4.0 license (http://creativecommons.org/licenses/by-nc-nd/4.0/).

Cite This: *JUSTC*, **2022**, 52(8): 6 (7pp)

Read Online

SI Supporting Information

Abstract: A three-dimensional elastic carbon nanotube aerogel is fabricated via a simple solution-based strategy using Te nanowires as templates, which can be recycled. The pipe diameter and wall thickness of the carbon nanotube are strongly dependent on the diameter of the Te nanowires and carbon source. The obtained free-standing carbon nanotube aerogel with a large specific surface area (up to 1865 $m^2 \cdot g^{-1}$) is promising as an electrode material for supercapacitors. After combination with MnO_2, the capacitor exhibits a specific capacitance of 360.4 $F \cdot g^{-1}$ at a current of 1 $A \cdot g^{-1}$ and retention of 97% after 2000 cycles. The high power capabilities and good stability make it a promising candidate as an electrode for supercapacitors.

Keywords: carbon nanotube aerogel; MnO_2; specific surface area; supercapacitor

CLC number: O648.17 **Document code:** A

1 Introduction

In recent decades, the application of carbon materials as electrode materials for electrochemical capacitors and Li-ion batteries has attracted considerable interest owing to their excellent electrical conductivities, large surface areas, chemical stability, simple processing, and relatively low cost[1–8]. Various carbon materials are used as electrode materials, including activated carbons (ACs)[9–13], carbon nanotubes[14–18], template carbons[19, 20], and graphene[21–25].

ACs are the mostly widely used electrode materials because of their large surface areas and relatively good electrical properties. However, their large pore volumes lead to low material densities and conductivities, and thus to low volumetric energy densities and loss of power capability. In addition, the large active surface areas may increase the risk of decomposition of the electrolyte at the active spot positions.

Carbon nanotubes, owing to their unique pore structures, superior electrical properties, and good mechanical and thermal stabilities, have attracted considerable attention for supercapacitor electrode applications. Despite the excellent properties, the limited surface area of carbon nanotubes restricts their use as high-energy-performance electric double-layer capacitors. In addition, the difficulties in purification and high cost of production hinder their practical applications[26]. The templating method is effective in producing carbon nanostructures with well-controlled narrow pore size distributions, ordered pore structures, large specific surface areas, and interconnected pore network, making them promising candidates for supercapacitor electrode materials.

To address these problems, a simple solution-based strategy is introduced to prepare a bifunctional carbon nanotube aerogel with controllable pipe diameter and wall thickness, which serves as a promising electrode material without binding substances for high-rate electrochemical capacitor applications. This bifunctional and elastic carbon nanotube aerogel is fabricated via a simple hydrothermal-carbonization process using Te nanowires (Te NWs) as a template, exhibiting a large number of micropores (<1 nm) and mesopores (>2 nm and <50 nm), followed by a high-temperature annealing to obtain the large-specific-surface-area carbon nanotube aerogel (up to 1865 $m^2 \cdot g^{-1}$).

2 Materials and methods

2.1 Materials

Sodium tellurite (99%), poly(vinyl pyrrolidone) (PVP, M_W = 30000), acetone (99%), ethylene glycol (99%), hydrazine hydrate (85%), ammonia (25%–28%), and glucose (99%) were purchased from Shanghai Reagent Company (China). All chemicals were used without further purification.

2.2 Synthesis of Te NWs with different diameters

In a typical synthesis, 0.9220 g of Na_2TeO_3 and 10 g of PVP were dissolved in 280, 230, 180, and 150 mL of ethylene glycol and 50, 100, 150, and 180 mL of acetone, and then 16.5 mL of hydrazine hydrate and 33.5 mL of ammonia solution were added and stirred at room temperature under strongly magnetic conditions to form a homogeneous solution. The solution was then transferred to a 500 mL Teflon-lined stainless-steel autoclave, sealed, and heated at 180 ℃ for 3 h, which yielded Te NWs with average diameters of 10, 20, 40, and 80 nm.

DOI: 10.52396/JUSTC-2022-0065

JUSTC, **2022**, 52(8): 6

2.3 Synthesis of carbon nanotube gels

The carbon nanotube gel was templated with Te NWs. 380 mL of the Te NW solution was settled down with 750 mL of acetone, and then the Te NWs were dissolved in 40 mL of deionized water. 2.5 g of glucose was then added to the aqueous solution of the above Te NWs and magnetically stirred at room temperature for 15 min. The carbon nanotube hydrogel was obtained by reaction in a 50 mL reactor at 180 ℃ for 24 h. The hydrogel was soaked in ethanol to remove impurities, and then supercritically dried to obtain the precursor of the carbon nanotube gel. The carbon nanotube gel was obtained by heating at 900 ℃ for 2 h in an inert gas atmosphere.

2.4 Fabrication of supercapacitors

The carbon nanotube gel was cut into 1.0 cm × 1.0 cm thin slices with a thickness of 1.0 mm. Two sheets of the same quality were taken and soaked in 1 mol·L^{-1} of H_2SO_4 for 1 h. A platinum sheet was used as a current collector. The capacitor was assembled by the two-electrode method and placed in a 1 mol·L^{-1} H_2SO_4 solution for testing.

2.5 Fabrication of Li-ion batteries

The carbon nanotube gel was cut into slices with a diameter of 10 mm and thickness of 1.5 mm. The carbon nanotube flakes were then dried in a vacuum drying oven at 80 ℃ and placed in a glove box for battery assembly. The inside of the glove box was an argon atmosphere. The concentrations of water and oxygen should be controlled below 0.1 ppm. A half-cell was assembled using a lithium sheet as a positive electrode, glass fiber purchased from Whatman as a separator, and $LiPF_6$ as an electrolyte.

2.6 Characterization

Scanning electron microscopy (SEM) images were acquired using a Zeiss Supra 40 microscope at an accelerating voltage of 5 kV. Transmission electron microscopy (TEM) images were acquired using a Hitachi H7650 microscope operating at an accelerating voltage of 120 kV using a charge-coupled device imaging system. Energy-dispersive spectroscopy (EDS) and high-resolution (HR) TEM measurements were carried out using a JEM-ARM 200F transmission electron microscope at an accelerating voltage of 200 kV. X-ray diffraction (XRD) was carried out using a Philips X'Pert Pro Super diffractometer equipped with a graphite monochromatic Cu K_α radiation (λ = 1.54056 Å). A thermogravimetric analysis (TGA) was carried out using a Perkin Elmer Diamond TG/DTA instrument at a heating rate of 10 ℃·min^{-1} and nitrogen flow rate of 50 mL·min^{-1}. X-ray photoelectron spectroscopy (XPS) was carried out using an ESCALAB-MK-II X-ray instrument with Mg K_a rays (1.2536 eV).

2.7 Electrochemical characterization

Cyclic voltammetry (CV) curves were measured at different scan rates using a CHI 760D electrochemical workstation. Galvanostatic charge–discharge curves were measured at different current densities. The impedance was measured in the range of 10 mHz to 100 kHz at a full current amplitude of 5 mV. CV curves of the cells were measured using an Autolab PG302N in a voltage range of 0.1–3.0 V at a scan rate of 0.05 mV·s^{-1}. Cycling performance curves of the batteries were measured using an Arbin BT-1 system.

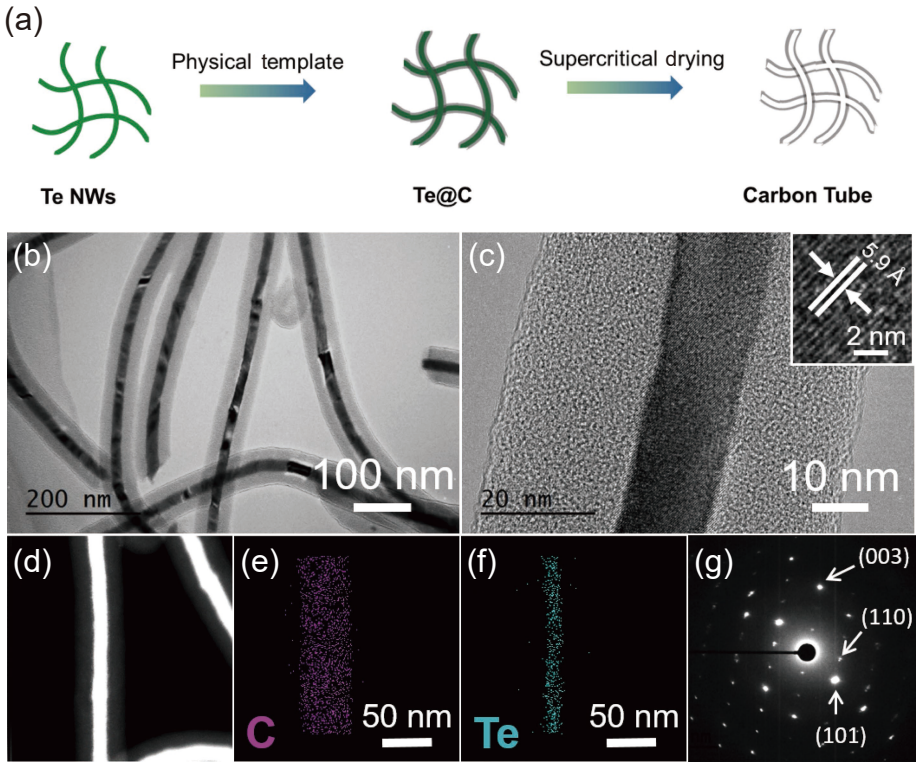


Fig. 1. (a) Schematic of the typical synthesis of the carbon tube. (b,c) TEM images of the Te@C fiber (Te NWs coated with a uniform carbon shell) at different magnifications. The inset of (c) shows a HRTEM image of the inner Te NW. (d–f) Maps of the Te@C nanocable. (g) Corresponding selected-area electron diffraction pattern of a Te@C nanowire cable.

DOI: 10.52396/JUSTC-2022-0065
JUSTC, **2022**, 52(8): 6

3 Results and discussion

Fig. 1a shows the preparation steps of carbon tubes. Using Te nanowires as sacrificial templates, the hollow carbon nanotubes were synthesized via hydrothermal and carbonization process. The structure of Te@C nanocables was investigated by TEM. As shown in Fig. 1b, Te NW was coated with a uniform carbon shell. Fig. 1c shows the HRTEM image of Te@C nanocables. The inset shows that the lattice spacing is 5.9 Å. From the elemental mapping of Te@C nanocables (Fig. 1d–f), the structure of Te@C was successfully synthesized, and the elements of Te and C were uniformly distributed in the inner and outer, respectively. The corresponding selected-area electron diffraction pattern of a Te@C nanowire cable(Fig. 1g) shows the lattice of the (110), (101), (003) planes，further confirming the crystal structure.

The specific surface area of a carbon material is mainly determined by the number and size of the aperture. To prepare carbon nanotube aerogels with different inradium, we start with the synthesis of ultrathin Te NWs with different diameters as a sacrificial template (Fig. 2a–d). The synthetic method of Te NWs with different diameters is shown in Supporting information[27]. Their purity is confirmed by SEM images (Fig. S1) and XRD patterns (Fig. S4a). A simple hydrothermal process was employed to coat a uniform carbon precursor shell onto the Te NWs. Fig. 2e,f show that the thickness of the tube wall decreases when the diameter of the Te NWs increases. The smallest thickness of the tube wall was 2 nm (Fig. S2). We could precisely control the thickness of the tube wall by adding different quantities of glucose. We used Te-40 as a template and added different quantities of glucose. We obtained a series of carbon nanotubes with thicknesses of the tube wall of 10 to 80 nm (Fig. S3). After the carbon nanotubes were dried by supercritical carbon dioxide ($scCO_2$), a high-temperature (800 ℃) annealing was carried out for carbon precursor shell carbonization. Simultaneously, the Te template was removed because the melting point of Te (452 ℃) is considerably below the carbonation temperature. The XRD pattern of the carbon nanotubes demonstrates that the Te element was completely removed (Fig. S4b).

The electrochemical capacitive performances of our free-standing carbon nanotube aerogel (1.0 cm× 1.0 cm) without any binder or conductive agent were evaluated in a 1.0 mol·L^{-1} H_2SO_4 aqueous electrolyte using a two-electrode system. Typical CV curves at 50 and 100 mV·s^{-1} for all samples are shown in Fig. 3. The CV curves in Fig. 3a,b show that the carbon nanotube-*x* (*x* = 10, 20, 40, 80) exhibits a nearly rectangular curve at a potential scan rate of 50 mV·s^{-1} and even at a high scan rate of 100 mV·s^{-1} though with a few humps because of the pseudocapacitive process. The largest rectangle area separated from the CV curve represents the electrical double-layer (EDL) capacitance, while the remaining part corresponds to the pseudocapacitance. According to the CV curves of the carbon nanotube-*x* (*x* = 10, 20, 40, 80), the EDL capacitance increased with the inradium owing to the effective specific surface area. We evaluated the specific surface area of the carbon nanotube-*x* (*x* = 10, 20, 40, 80) aerogel by the Brunauer-Emmett-Teller (BET) method. The carbon nanotube-*x* (*x* = 10, 20, 40, 80) aerogels exhibited combined N_2 adsorption/desorption isotherms, with large specific surface areas of 501.5, 508.6, 1864.6, and 1762.7 $m^2 \cdot g^{-1}$, respectively. The type-I adsorption and type-H2 hysteresis loop indicate micropores and mesopores, respectively (Fig. S5a). The pore size distribution obtained by the density functional theory method further confirms the hierarchically porous structure mainly consisting of micropores (<1 nm) and mesopores (depending on the tube diameter of the carbon nanotube) in a pore width range of 0.4–130 nm (Fig. S5b). According to the BET test, the carbon nanotube-40 exhibited the largest specific surface area, which may be attributed to the large number of micropores (~0.6 nm) and large-scale mesopores (~2, 40, 80 nm) (Fig. S5b). In contrast to the carbon nanotube-40, the

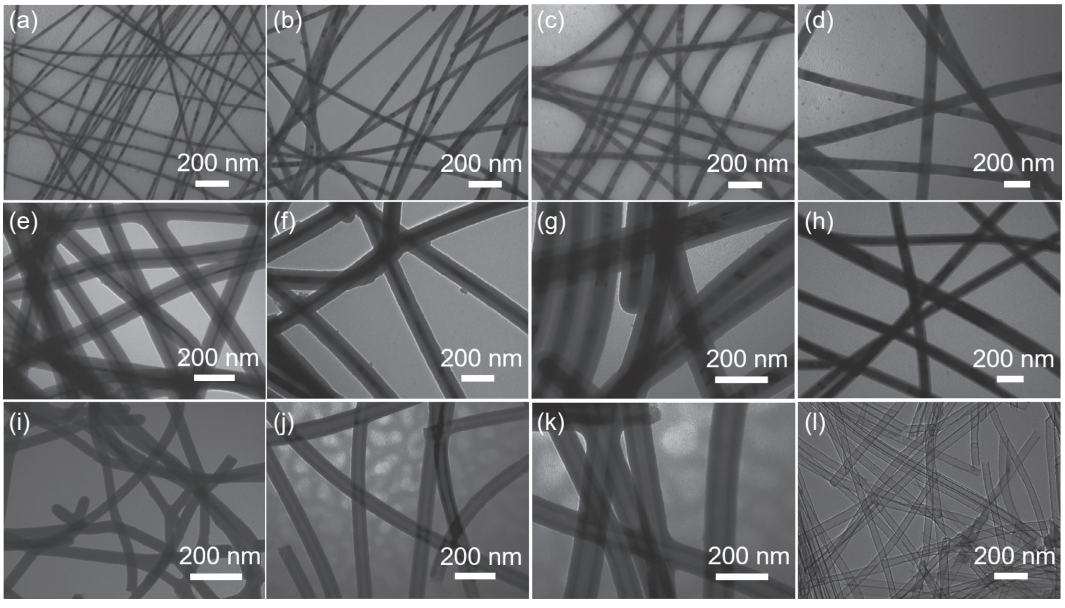


Fig. 2. Morphology control of the tubular carbon aerogel. (a–d) TEM images of Te NWs with different diameters of 10, 20, 40, 80 nm, respectively. (e,f) TEM images of the Te@C fibers obtained with Te NWs with different diameters as templates. (i–l) TEM images of the carbon nanotubes with different pipe diameters and wall thicknesses obtained using the Te@C precursor (e,f) by a high-temperature annealing.

DOI: 10.52396/JUSTC-2022-0065
JUSTC, **2022**, 52(8): 6

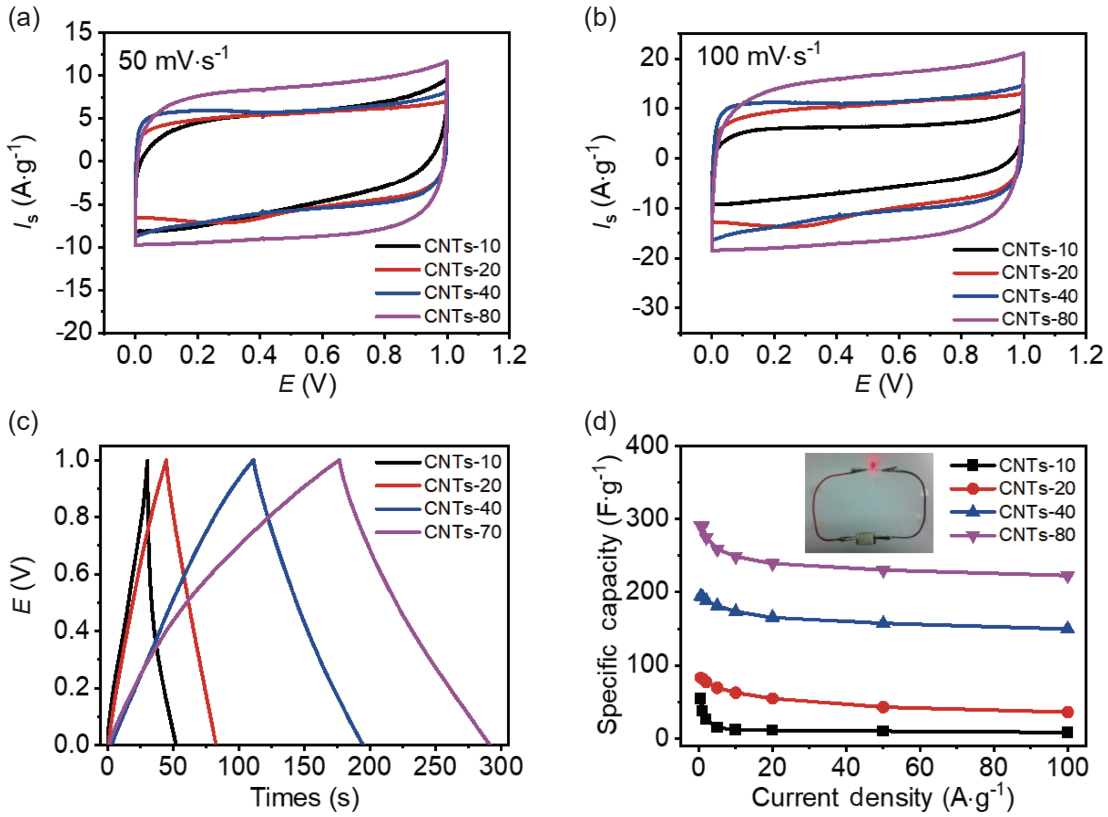


Fig. 3. Electrochemical performances measured in a two-electrode system. Cyclic voltammograms of the carbon nanotube-10, carbon nanotube-20, carbon nanotube-40, and carbon nanotube-80 at scan rates of (a) 50 mV·s^{-1} and (b) 100 mV·s^{-1}. (c) Galvanostatic charge–discharge curves at 1 A·g^{-1}. (d) Volumetric capacitances at different current densities.

carbon nanotube-10 and carbon nanotube-20 almost do not have mesopores, which could be attributed to the small tube diameter. The lack of micropores in the carbon nanotube-80 may be attributed to the too small wall thickness. Hence, we developed a simple and rapid template method to produce a carbon nanotube aerogel. A considerable improvement in the specific surface area of the carbon nanotube aerogel was achieved, making it a promising candidate for electrode materials of supercapacitors.

To demonstrate that the inradium has an important influence on the performances of the supercapacitors, we employed the galvanostatic charge–discharge method, a more reasonable method than the CV test for the determination of the specific capacitance. We carried out galvanostatic charge–discharge tests at various current densities. Fig. 3c shows that the discharge time increased with the change from the carbon nanotube-10 film to the carbon nanotube-80 film, which agrees with the above CV tests. The gravimetric capacitances of the carbon nanotube-10, 20, 40, 80 films at 1 A·g^{-1} are 37.3, 81.6, 193.2, and 290.5 F·g^{-1}, respectively. The galvanostatic charge–discharge curves of the carbon nanotube-10, 20, 40, 80 at different current densities are shown in Fig. S6.

The gravimetric capacitance of the carbon nanotube-80 film was improved by a factor of approximately 8 compared to that of the carbon nanotube-10. The carbon nanotube-80 had the highest capacitance mainly owing to the thin wall, which makes the transport of ions smoother. A perfect supercapacitor should deliver the same energy under any operation conditions. Thus, it is important to investigate the capacitance retention at higher current densities. The relationships between the specific capacity and charge/discharge current density measured in a two-electrode system are presented in Fig. 3d. Slight decreases in the specific capacities of the carbon nanotube-20, 40, 80 were observed as the current density increased from 0.5 to 100.0 A·g^{-1}, which indicates that this electrode material exhibits a good capacitance retention capability. The specific capacity of the carbon nanotube-80 at 10.0 A·g^{-1} was 249.0 F·g^{-1}, ~85.7% of the value at 1.0 A·g^{-1}, which also shows that the specific capacitance of the carbon nanotube-x (x = 20, 40, 80) was not kinetically limited. The excellent retention capability, except that of the carbon nanotube-10, indicates that the suitable size distribution of the meso/micropores is beneficial for the formation of the electric double layer and improvement in the speed of ions in the electrolyte when the tube diameter of the carbon nanotube is not smaller than 20 nm. The charge–discharge profiles at current densities of 0.5 to 10 A·g^{-1} (Fig. S6) are almost linear and symmetrical, which also indicates a high Columbic efficiency.

Thus, our carbon nanotubes are suitable as a supercapacitor electrode. To demonstrate that this material can be used as a good matrix material and further improve the performance of the capacitors, we load MnO_2 on the surfaces of the carbon nanotube fibers. MnO_2 could be an excellent electrode material for supercapacitors because of its high specific capacitance, low cost, and environmental compatibility[28–33]. The SEM and TEM images in Fig. 4 show the MnO_2 uniform

DOI: 10.52396/JUSTC-2022-0065
JUSTC, **2022**, 52(8): 6

growth on the surface of the carbon nanotube fibers without granules. We also evaluated the electrochemical capacitive performances of MnO_2@carbon nanotube-40 in a two-electrode system. The typical CV curves in Fig. 5a at 50 and 100 $mV \cdot s^{-1}$ are as those of the carbon nanotube-*x* electrodes, with a higher gravimetric capacitance of 360.4 $F \cdot g^{-1}$ at 1 $A \cdot g^{-1}$. The specific capacity at 10.0 $A \cdot g^{-1}$ was 293.4 $F \cdot g^{-1}$, ~81.4% of the value at 1.0 $A \cdot g^{-1}$, which indicates that this electrode material

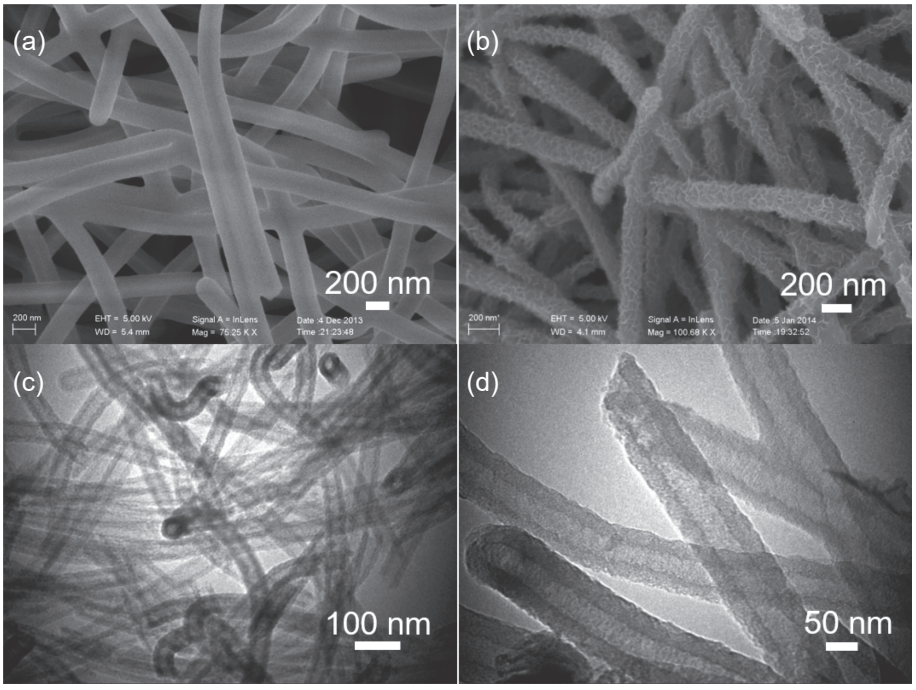


Fig. 4. (a) SEM image of the carbon nanotube-40. (b) SEM image of the MnO_2@carbon nanotube-40. (c) TEM image of the MnO_2@carbon nanotube-40. (d) TEM image of the MnO_2@carbon nanotube-40 at a high magnification.

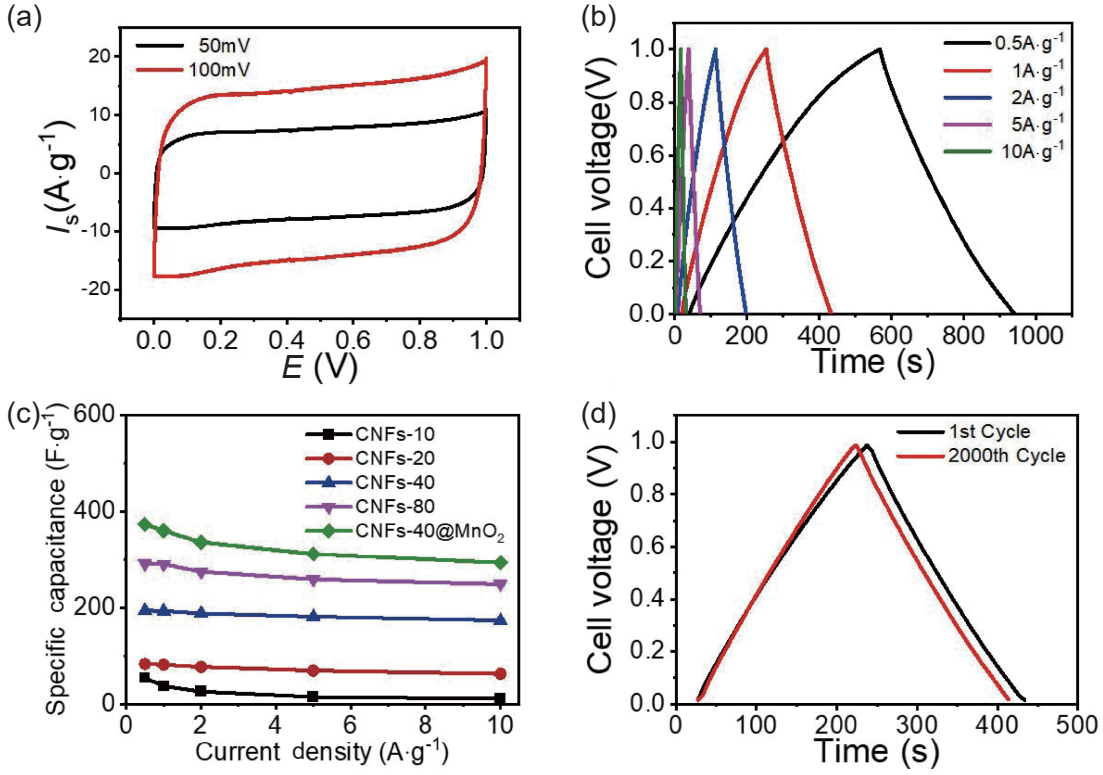


Fig. 5. Electrochemical performances measured in a two-electrode system. Cyclic voltammograms of the MnO_2@carbon nanotube-40 at scan rates of 50 and 100 $mV \cdot s^{-1}$. (b) Galvanostatic charge–discharge curves of the MnO_2@carbon nanotube-40 at different current densities. (c) Volumetric capacitances of the MnO_2@ carbon nanotube-40 and carbon nanotube-*x* (*x* = 10, 20, 40, 80) at different current densities. (d) Triangular shapes of the first and 2000th cycles.

DOI: 10.52396/JUSTC-2022-0065
JUSTC, **2022**, 52(8): 6

exhibits a good capacitance retention capability (Fig. 5b). Further, we studied the durability of the MnO_2@carbon nanotube-40 electrode to characterize the long-term charge/discharge behavior at a current density of 1.0 $A \cdot g^{-1}$ by a galvanostatic charge/discharge measurement. The triangular shape of the 2000th galvanostatic charge/discharge cycle, shown in Fig. 5d, shows that the specific capacitance is approximately 343.5 $F \cdot g^{-1}$ (above 95.3% of the initial capacitance). Thus, our carbon nanotubes can be used as a good supporter to carry other materials.

Table 1 compares our carbon nanotube gel supercapacitor's specific surface area, specific capacitance, and cycling performance to those of reported supercapacitors. The gel prepared in this study has a specific surface area largely exceeding those of other supercapacitors, which ensures an excellent specific capacity without complex modification and loading. In addition, it has an excellent cycling stability. The high power capacity and good stability make it a promising candidate for supercapacitor electrodes.

Table 1. Comparison of carbon-nanotube-based supercapacitors.

Ref.	Electrode materials	Specific surface area ($m^2 \cdot g^{-1}$)	Specific capacitance($F \cdot g^{-1}$)	Cycles	Cycling stability (%)
[34]	CNT / SS @ IL	—	329.13	1000	91.9
[34]	CNT@ IL	—	107.21	1000	81.6
[35]	CNT fibers	395	20.8	10000	98.3
[36]	CNT@CZIFs	287	324	1000	93.5
[37]	LCFA	580	300.1	5000	90
[38]	CNT-COOH（oPDA-1）	27.542	147.14	1000	82
This work	CNT-40 @ MnO_2	1865	360.4	2000	97

4 Conclusions

A bifunctional and elastic carbon nanotube aerogel was fabricated via a simple hydrothermal-carbonization process using the Te NWs as the sacrificial template. In addition, we synthesized different carbon nanotubes by Te NWs with diverse diameters, which can be used for electrodes of supercapacitors. We obtained different carbon nanotube aerogels with different parameters, which directly affected the specific surface area and pore size distribution. The unique characteristics of the hollow structure provided the carbon nanotube-80 with a better capacitive performance, high electrochemical capacitance of 290.5 $F \cdot g^{-1}$ at a current density of 1.0 $A \cdot g^{-1}$, good capacitance retention of ~85.7% at current densities up to 10 $A \cdot g^{-1}$, and good cycling stability up to 2000 cycles. The results demonstrate that the carbon nanotubes are very promising as alternative electrode materials for supercapacitors. We believe that this material can be used in various fields, such as electronic devices, catalysts, sensors, and hydrogen storage materials.

Supporting information

The supporting information for this article can be found online at https://doi.org/10.52396/JUSTC-2022-0065.

Acknowledgements

This work was partially carried out at the USTC Center for Micro and Nanoscale Research and Fabrication. This work was supported by the National Natural Science Foundation of China (21922204, 22175164, 21771168), the Joint Funds from Hefei National Synchrotron Radiation Laboratory (UN2018LHJJ) and University Synergy Innovation Program of Anhui Province, China (GXXT-2020-072).

Conflict of interest

The authors declare that they have no conflict of interest.

Biographies

Qiguo Shang is currently pursuing a master's degree at the University of Science and Technology of China. His research focuses on the assembly and functionalization of one-dimensional nanomaterials.

Jie Xu received his Ph.D. degree in Inorganic Chemistry from the University of Science and Technology of China in 2015. His research focuses mainly on the design, synthesis and properties of one-dimensional tellurium nanostructures.

Jianwei Liu received his Ph.D. degree in Inorganic Chemistry from the University of Science and Technology of China (USTC) in 2013. He is currently a faculty in the Department of Chemistry, USTC. His research focuses mainly on the synthesis and self-assembly of nanoscale building blocks as well as their derived nanodevices.

References

[1] Zhai Y P, Dou Y Q, Zhao D Y, et al. Carbon materials for chemical capacitive energy storage. *Adv. Mater.*, **2011**, *23* (42): 4828–4850.
[2] Zhu Y, Murali S, Stoller M D, et al. Carbon-based supercapacitors produced by activation of graphene. *Science,* **2011**, *332* (6037): 1537–1541.
[3] Zhou D, Cui Y, Han B H. Graphene-based hybrid materials and their applications in energy storage and conversion. *Chin. Sci. Bull.,* **2012**, *57* (23): 2983–2994.
[4] Zheng G Y, Lee S W, Liang Z, et al. Interconnected hollow carbon nanospheres for stable lithium metal anodes. *Nat. Nanotechnol.,* **2014**, *9* (8): 618–623.
[5] Lou X W, Archer L A, Yang Z. Hollow micro-/nanostructures: Synthesis and applications. *Adv. Mater.,* **2008**, *20* (21): 3987–4019.
[6] Liu C, Li F, Ma L P, et al. Advanced materials for energy storage. *Adv. Mater.,* **2010**, *22* (8): E28–E62.
[7] Li H, Wang Z X, Chen L Q, et al. Research on advanced materials for Li-ion batteries. *Adv. Mater.,* **2009**, *21* (45): 4593–4607.
[8] Arico A S, Bruce P, Scrosati B, et al. Nanostructured materials for advanced energy conversion and storage devices. *Nat. Mater.,* **2005**, *4* (5): 366–377.
[9] Yu X W, Manthiram A. Ambient-temperature sodium-sulfur batteries with a sodiated Nafion membrane and a carbon nanofiber-

DOI: 10.52396/JUSTC-2022-0065
JUSTC, **2022**, 52(8): 6

activated carbon composite electrode. *Adv. Energy. Mater.,* **2015**, *5* (12): 1500350.
[10] McDonough J R, Choi J W, Yang Y, et al. Carbon nanofiber supercapacitors with large areal capacitances. *Appl. Phys. Lett.,* **2009**, *95* (24): 243109.
[11] Kim T, Jung G, Yoo S, et al. Activated graphene-based carbons as supercapacitor electrodes with macro- and mesopores. *ACS Nano,* **2013**, *7* (8): 6899–6905.
[12] Kim H, Cho M Y, Kim M H, et al. A novel high-energy hybrid supercapacitor with an anatase TiO_2-reduced graphene oxide anode and an activated carbon cathode. *Adv. Energy. Mater.,* **2013**, *3* (11): 1500–1506.
[13] Wang G M, Wang H Y, Lu X H, et al. Solid-state supercapacitor based on activated carbon cloths exhibits excellent rate capability. *Adv. Mater.,* **2014**, *26* (17): 2676–2682.
[14] Kaempgen M, Chan C K, Ma J, et al. Printable thin film supercapacitors using single-walled carbon nanotubes. *Nano Lett.,* **2009**, *9* (5): 1872–1876.
[15] Futaba D N, Hata K, Yamada T, et al. Shape-engineerable and highly densely packed single-walled carbon nanotubes and their application as super-capacitor electrodes. *Nat. Mater.,* **2006**, *5* (12): 987–994.
[16] Frackowiak E, Beguin F. Electrochemical storage of energy in carbon nanotubes and nanostructured carbons. *Carbon,* **2002**, *40* (10): 1775–1787.
[17] De Volder M F L, Tawfick S H, Baughman R H, et al. Carbon nanotubes: Present and future commercial applications. *Science,* **2013**, *339* (6119): 535–539.
[18] Che G L, Lakshmi B B, Fisher E R, et al. Carbon nanotubule membranes for electrochemical energy storage and production. *Nature,* **1998**, *393* (6683): 346–349.
[19] Wang D W, Li F, Liu M, et al. 3D aperiodic hierarchical porous graphitic carbon material for high-rate electrochemical capacitive energy storage. *Angew. Chem. Int. Ed.,* **2007**, *47* (2): 373–376.
[20] Cheng F Y, Tao Z L, Liang J, et al. Template-directed materials for rechargeable lithium-ion batteries. *Chem. Mater.,* **2008**, *20* (3): 667–681.
[21] Yoo E, Kim J, Hosono E, et al. Large reversible Li storage of graphene nanosheet families for use in rechargeable lithium ion batteries. *Nano Lett.,* **2008**, *8* (8): 2277–2282.
[22] Wang D, Choi D, Li J, et al. Self-assembled TiO_2-graphene hybrid nanostructures for enhanced Li-ion insertion. *ACS Nano,* **2009**, *3* (4): 907–914.
[23] Chen S, Zhu J W, Wu X D, et al. Graphene oxide-MnO_2 nanocomposites for supercapacitors. *ACS Nano,* **2010**, *4* (5): 2822–2830.
[24] Reddy A L M, Srivastava A, Gowda S R, et al. Synthesis of nitrogen-doped graphene films for lithium battery application. *ACS Nano,* **2010**, *4* (11): 6337–6342.
[25] Wu Z S, Ren W C, Xu L, et al. Doped graphene sheets as anode materials with superhigh rate and large capacity for lithium ion batteries. *ACS Nano,* **2011**, *5* (7): 5463–5471.
[26] Zhang L L, Zhao X S. Carbon-based materials as supercapacitor electrodes. *Chem. Soc. Rev.,* **2009**, *38* (9): 2520–2531.
[27] Qian H S, Yu S H, Gong J Y, et al. High-quality luminescent tellurium nanowires of several nanometers in diameter and high aspect ratio synthesized by a poly (vinyl pyrrolidone)-assisted hydrothermal process. *Langmuir,* **2006**, *22* (8): 3830–3835.
[28] Liang H W, Wang L, Chen P Y, et al. Carbonaceous nanofiber membranes for selective filtration and separation of nanoparticles. *Adv. Mater.,* **2010**, *22* (42): 4691–4695.
[29] Fan Z J, Yan J, Wei T, et al. Asymmetric supercapacitors based on graphene/MnO_2 and activated carbon nanofiber electrodes with high power and energy density. *Adv. Funct. Mater.,* **2011**, *21* (12): 2366–2375.
[30] Wei W, Cui X, Chen W, et al. Manganese oxide-based materials as electrochemical supercapacitor electrodes. *Chem. Soc. Rev.,* **2011**, *40* (3): 1697–1721.
[31] Yu G, Hu L, Vosgueritchian M, et al. Solution-processed graphene/MnO_2 nanostructured textiles for high-performance electrochemical capacitors. *Nano Lett.,* **2011**, *11* (7): 2905–2911.
[32] Wu Z S, Ren W C, Wang D W, et al. High-energy MnO_2 nanowire/graphene and graphene asymmetric electrochemical capacitors. *ACS Nano,* **2010**, *4* (10): 5835–5842.
[33] Guo C X, Wang M, Chen T, et al. A hierarchically nanostructured composite of MnO_2/conjugated polymer/graphene for high-performance lithium ion batteries. *Adv. Energy. Mater.,* **2011**, *1* (5): 736–741.
[34] Lyu X M, Su F H, Miao M H. Two-ply yarn supercapacitor based on carbon nanotube/stainless steel core-sheath yarn electrodes and ionic liquid electrolyte. *J. Power Sources,* **2016**, *307*: 489–495.
[35] He S S, Hu Y J, Wan J X, et al. Biocompatible carbon nanotube fibers for implantable supercapacitors. *Carbon,* **2017**, *122*: 162–167.
[36] Wan L, Shamsaei E, Easton C D, et al. ZIF-8 derived nitrogen-doped porous carbon/carbon nanotube composite for high-performance supercapacitor. *Carbon,* **2017**, *121*: 330–336.
[37] Rong K, Wei J L, Wang Y C, et al. Deep eutectic solvent assisted zero-waste electrospinning of lignin fiber aerogels. *Green Chem.,* **2021**, *23* (16): 6065–6075.
[38] Chakraborty S, Simon R, Vadakkekara A, et al. Microwave assisted synthesis of poly(ortho-phenylenediamine-co-aniline) and functionalised carbon nanotube nanocomposites for fabric-based supercapacitors. *Electrochim. Acta,* **2022**, *403*: 139678.

DOI: 10.52396/JUSTC-2022-0065
JUSTC, **2022**, 52(8): 6